

# Towards human Super EEG

Lucy L. W. Owen<sup>1</sup>, Andrew C. Heusser<sup>1,2</sup>, and Jeremy R. Manning<sup>1\*</sup>

<sup>1</sup>Department of Psychological and Brain Sciences, Dartmouth College,  
Hanover, NH 03755, USA

<sup>2</sup>Akili Interactive,  
Boston, MA 02110, USA

## Abstract

A growing body of literature over the past several decades reports that the dynamic correlational structure of functional neuroimaging data may be used to predict which moment of movie or story an individual is experiencing, identify which person's brain a recording came from, and identify the task a person is performing. However, our structural (anatomical) connectome is roughly static for the duration of typical neuroimaging experiments. How might these notions of dynamic functional connectomes versus static structural connectomes be reconciled? We use two human electrocorticographic (ECoG) datasets to ask: to what extent can we use a static connectome model (trained using within versus across subject data, and within versus across task data) to explain dynamic full-brain activity patterns? Given a fixed connectome model, and given recordings from a subset of brain locations, we test how reliably can one infer activity patterns throughout the rest of the brain. Our model-based approach, termed *SuperEEG*<sup>1</sup>, is in itself useful for inferring full-brain activity patterns (at millimeter-scale spatial resolutions and millisecond-scale temporal resolutions) from ECoG recordings from a limited set of brain locations. For both datasets, we found that full-brain activity patterns can be best explained using connectomes from *other* people who performed a shared task.

**Keywords:** Electrocorticography (ECoG), intracranial electroencephalography (iEEG), local field potential (LFP), epilepsy, maximum likelihood estimation, Gaussian process regression

Are our brain's networks static or dynamic? And to what extent are the network properties of our brains stable across people and tasks? One body of work suggests that our brain's func-

<sup>1</sup>The term "Super EEG" was coined by Robert J. Sawyer in his popular science fiction novel *The Terminal Experiment* [20]

*tional* networks are dynamic [e.g., 16], person-specific [e.g., 5], and task-specific [e.g., 28]. In contrast, although the gross anatomical structure of our brains changes meaningfully over the course of years as our brains develop, on the timescales of typical neuroimaging experiments (i.e., hours to days) our anatomical networks are largely stable [e.g., 2]. Further, many aspects of brain anatomy, including white matter structure, is largely preserved across people [e.g., 7, 18, 27] There are several possible means of reconciling this apparent contradiction between dynamic person- and task-specific functional networks versus stable anatomical networks. For example, relatively small magnitude anatomical differences across people may be reflected in reliable functional connectivity differences. Along these lines, one recent study found that diffusion tensor imaging (DTI) structural data is similar across people, but may be used to predict person-specific resting state functional connectivity data [1]. Another (potentially complementary) possibility is that our functional networks are constrained by anatomy, but nevertheless exhibit rapid task-dependent changes [e.g., 26].

Here we take a model-based approach to studying whether high spatiotemporal resolution activity patterns throughout the human brain may be explained by a static connectome model that is shared across people and tasks. Specifically, we trained a model to take in recordings from a subset of brain locations, and then predict activity patterns during the same interval, but at *other* locations that were held out from the model. Our model, based on Gaussian process regression, relies on three assumptions (each of which we test). First, we assume that functional correlations are stable over time and across tasks. Second, we assume that some of the correlational structure of people’s brain activity is similar across individuals. Third, we resolve ambiguities in the data by assuming that neural activity from nearby sources will tend to be similar, all else being equal. After fitting the model to an ECoG dataset, one can then ask (for a held-out individual’s brain): given what we know about the correlational structure of *other* people’s brains, and given the recordings we made from electrodes implanted in this person’s

51 brain, how would those recordings most likely have looked at *other* locations throughout this  
52 person’s brain? We named our general approach *SuperEEG* because the trained model provides  
53 a means of inferring full-brain activity patterns at high spatiotemporal resolutions, using ECoG  
54 recordings taken from a limited set of brain locations.

55 We tested the SuperEEG approach using two large ECoG datasets. Dataset 1 comprises  
56 multi-hour recordings from 6876 electrodes taken across several recording sessions as 88 neu-  
57 rosurgical patients studied random word lists periodically throughout their day [13, 15, 21–23].  
58 Dataset 2 comprises recordings from XXX electrodes taken as XXX patients performed a se-  
59 ries of two memory tasks [3, 4, 6, 8–11, 25, 29]. In both datasets, we compared the predictions  
60 made using models trained across people to predictions made using within-person data. We  
61 found that models that incorporate data from other patients yield far more reliable predictions  
62 about an individual patient’s brain activity patterns than models trained solely on that individ-  
63 ual’s data. This indicates that at least some functional correlations are common across people.  
64 We also used Dataset 2 to compare predictions made using data from within task, across task,  
65 or combining within and across task data. We found that all three approaches yielded reli-  
66 able predictions, but the within task predictions were the most accurate. This indicates that  
67 some aspects of our functional connectomes are common across tasks, whereas other aspects  
68 are task-specific. Finally, all of the models we trained (within and across patients and tasks)  
69 assumed a static connectome and yielded above-chance accuracy. This indicates that despite  
70 moment-by-moment fluctuations in the functional connectome, at least some aspects of our  
71 connectome appear to be stable over the course of several hours.

72 **JRM STOPPED HERE**

73 **Approach**

74 The SuperEEG approach to inferring high temporal resolution full-brain activity patterns is  
75 outlined and summarized in Figure 1. We describe (in this section) and evaluate (in *Results*)  
76 our approach using a two large previously collected dataset comprising multi-session intracra-  
77 nial recordings. The first dataset was taken from 6876 electrodes implanted in the brains of  
78 88 epilepsy patients [13, 15, 21–23]. We first applied a fourth order Butterworth notch filter  
79 to remove 60 Hz ( $\pm .5$  Hz) line noise. We then excluded any electrodes that showed putative  
80 epileptiform activity. Specifically, we excluded from further analysis any electrode that exhib-  
81 ited an average kurtosis of 10 or greater across all of that patient’s recording sessions. We also  
82 excluded any patients with fewer than 2 electrodes that passed this criteria, as the Super EEG  
83 algorithm requires measuring correlations between 2 or more electrodes from each patient. Al-  
84 together this yielded clean recordings from 4168 electrodes implanted throughout the brains of  
85 67 patients (Fig. 1A). For the purposes of comparing task-specific contributions to reconstruc-  
86 tion accuracy, we limited our analyses in the second dataset to patients that participated in two  
87 free recall experiments. Applying the same kurtosis thresholding yielded clean recordings from  
88 24 patients and 2975 electrodes for the second dataset. Each individual patient contributes elec-  
89 trodes from a limited set of brain locations, which we localized in a common space (MNI152);  
90 an example patient’s 54 electrodes that passed the predefined kurtosis test are highlighted in  
91 black and red.

92 The recording from a given electrode is maximally informative about the activity of the  
93 neural tissue immediately surrounding its recording surface. However, brain regions that are  
94 distant from the recording surface of the electrode also contribute to the recording, albeit (often)  
95 to a much lesser extent. One mechanism underlying these contributions is volume conduction.  
96 The precise rate of falloff due to volume conduction (i.e. how much a small volume of brain

97 tissue at location  $x$  contributes to the recording from an electrode at location  $\eta$ ) depends on  
 98 the size of the recording surface, the electrode's impedance, and the conductance profile of the  
 99 volume of brain between  $x$  and  $\eta$ . As an approximation of this intuition, we place a Gaussian  
 100 radial basis function (RBF) at the location  $\eta$  of each electrode's recording surface (Fig. 1B). We  
 101 use the values of the RBF at any brain location  $x$  as a rough estimate of how much structures  
 102 around  $x$  contributed to the recording from location  $\eta$ :

$$\text{rbf}(x|\eta, \lambda) = \exp \left\{ -\frac{\|x - \eta\|^2}{\lambda} \right\}, \quad (1)$$

103 where the width variable  $\lambda$  is a parameter of the algorithm (which may in principle be set accord-  
 104 ing to location-specific tissue conductance profiles) that governs the level of spatial smoothing.  
 105 In choosing  $\lambda$  for the analyses presented here, we sought to maximize spatial resolution (which  
 106 implies a small value of  $\lambda$ ) while also maximizing the algorithm's ability to generalize to any  
 107 location throughout the brain, including those without dense electrode coverage (which implies  
 108 a large value of  $\lambda$ ). Using our prior work as a guide [14], we set  $\lambda = 20$ , although this could in  
 109 theory be optimized, e.g. using cross validation.

110 A second mechanism whereby a given region  $x$  can contribute to the recording at  $\eta$  is  
 111 through anatomical connections between structures near  $x$  and  $\eta$ . We use spatial correlations  
 112 in the data to estimate these anatomical connections. Let  $\bar{R}$  be the set of locations at which  
 113 we wish to estimate local field potentials, and let  $R_s$  be set of locations at which we observe  
 114 local field potentials from patient  $s$  (excluding the electrodes that did not pass the kurtosis test  
 115 described above). In the analyses below we define  $\bar{R} = \cup_{s=1}^S R_s$ . We can calculate the expected  
 116 inter-electrode correlation matrix for patient  $s$ , where  $C_{s,k}(i, j)$  is the correlation between the  
 117 time series of voltages for electrodes  $i$  and  $j$  from subject  $s$  during session  $k$ , using:

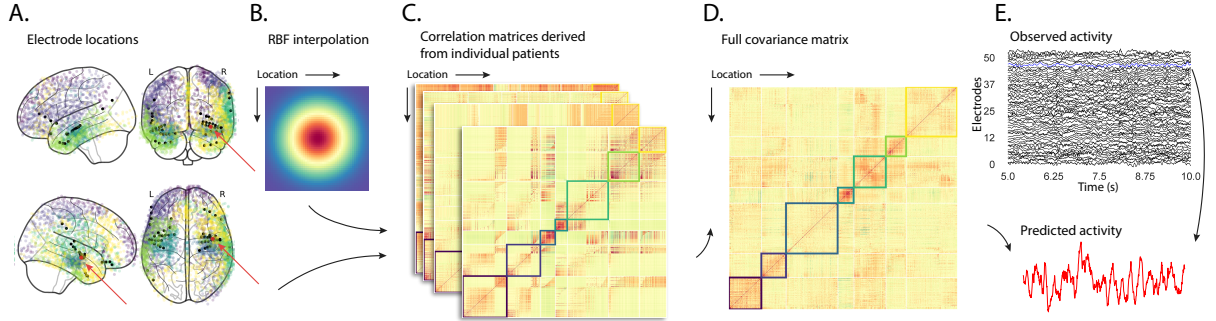


**Figure 1: Methods overview.** **A. Electrode locations.** Each dot reflects the location of a single electrode in dataset 1, colored according to 7 factor labels (see Panel D for details). One patient’s electrode locations are highlighted in black and the to-be-reconstructed recording location is highlighted in red. **B. Radial basis function (RBF).** Each electrode contributed by the patient (black) weights on the full set of locations under consideration (all dots in Panel A, defined as  $\bar{R}$  in the text). The weights fall off with positional distance (in MNI space) according to an RBF. **C. Per-patient correlation matrices.** After computing the pairwise correlations between the recordings from each patient’s electrodes, we use RBF-weighted averages to estimate correlations between all locations in  $\bar{R}$ . We obtain an estimated full-brain correlation matrix using each patient’s data. **D. Combined correlation matrix.** We estimate a single full-brain correlation matrix by averaging the patient-specific correlation matrices. We sort the resulting correlation matrix based on 7 factor labels obtained from k-means clustering [30]). **E. Reconstructing activity throughout the brain.** Given the observed activity from the patient’s electrodes and the estimated correlation matrix (Panel D), we can compute a maximum likelihood estimate of the voltage trace at any location in  $\bar{R}$ . An example reconstruction (at the red dot in Panel A) is shown in red, and the actual recording at that location is highlighted above in blue.

$$\bar{C}_s = r\left(\frac{1}{n}\left(\sum_{k=1}^n z(C_{s,k})\right)\right), \text{ where} \quad (2)$$

$$z(r) = \frac{\log(1+r) - \log(1-r)}{2} \text{ is the Fisher } z\text{-transformation and} \quad (3)$$

$$z^{-1}(z) = r(z) = \frac{\exp(2z) - 1}{\exp(2z) + 1} \text{ is its inverse.} \quad (4)$$

118 Next, we use Equation 1 to construct a number of to-be-estimated locations by number of pa-  
 119 tient electrode locations weight matrix,  $W$ . Specifically,  $W$  approximates how informative the  
 120 recordings at each location in  $R_s$  are in reconstructing activity at each location in  $\bar{R}$ , where  
 121 the contributions fall off with an RBF according to the distances between the corresponding  
 122 locations:

$$W(i, j) = \text{rbf}(i|j, \lambda). \quad (5)$$

123 Given this weight matrix,  $W$ , and the observed inter-electrode correlation matrix for patient  
 124  $s$ ,  $\bar{C}_s$ , we can estimate the correlation matrix for all locations in  $\bar{R}$  (Fig. 1C) using:

$$\hat{N}_s(x, y) = \sum_{i=1}^{|R_s|} \sum_{j=1}^{i-1} W(x, i) \cdot W(y, j) \cdot z(\bar{C}_s(i, j)) \quad (6)$$

$$\hat{D}_s(x, y) = \sum_{i=1}^{|R_s|} \sum_{j=1}^{i-1} W(x, i) \cdot W(y, j). \quad (7)$$

125 Intuitively, we construct an estimated correlation matrix from each individual patient's data  
 126 (Fig. 1C) using Equations 6 & 7, then we sum across these estimates for  $S$  patients and divide  
 127 (see Equations 8) to obtain the expected correlation matrix,  $\hat{K}$  (Fig. 1D):

$$\hat{K} = r \left( \frac{\sum \hat{N}_s}{\sum \hat{D}_s} \right). \quad (8)$$

128 Now we can use the following intuition: given (i) the observed responses from a limited set of  
 129 locations in  $R_s$  ( $Y_s$ ) and (ii) how each location's responses relate to all other responses ( $\hat{K}$ ), we  
 130 can estimate the LFP data from patient  $s$ , for any arbitrary location in  $\bar{R}$  (Fig. 1E).

131 Let  $\alpha$  be the set of indices of patient  $s$ 's electrode locations in  $\bar{R}$ , and let  $\beta$  be the set of  
 132 indices of all other locations in  $\bar{R}$ . In other words,  $\beta$  reflects the locations in  $\bar{R}$  where we did  
 133 not observe a recording for patient  $s$  (these are the recording locations we will want to fill in  
 134 using Super EEG). We can sub-divide  $\hat{K}$  as follows:

$$\hat{K}_{\beta,\alpha} = \hat{K}(\beta, \alpha), \text{ and} \quad (9)$$

$$\hat{K}_{\alpha,\alpha} = \hat{K}(\alpha, \alpha). \quad (10)$$

135 Here  $\hat{K}_{\beta,\alpha}$  stores the correlations between the “unknown” activity at the locations in  $\beta$  and the  
 136 observed activity at the locations in  $\alpha$ , and  $\hat{K}_{\alpha,\alpha}$  stores the correlations between the observed  
 137 recordings (at the locations in  $\alpha$ ).

138 Let  $Y_{s,k,\alpha}$  be the number-of-timepoints ( $T$ ) by  $\text{length}(\alpha)$  matrix of (observed) voltages from  
 139 the electrodes in  $\alpha$  during session  $k$  from patient  $s$ . Then we can estimate the voltage from  
 140 patient  $s$ 's  $k^{th}$  session at the locations in  $\beta$  using [19]:

$$Y_{s,k,\beta} = ((\hat{K}_{\beta,\alpha} \cdot \hat{K}_{\alpha,\alpha}^{-1}) \cdot Y_{s,k,\alpha}^T)^T. \quad (11)$$

141 This equation is the foundation of the Super EEG algorithm. Whereas we observe the recordings  
 142 only at the locations in  $\alpha$ , Equation 11 allows us to estimate the recordings at all locations in  
 143  $\beta$ , which we can define *a priori* to include any locations we wish, throughout the brain. This  
 144 yields estimates of the time-varying voltages at *every* location in  $\bar{R}$ .

145 We designed our approach to be agnostic to electrode impedances, as electrodes that do not  
 146 exist do not have impedances. Therefore our algorithm recovers voltages in standard deviation

147 ( $z$ -scored) units rather than attempting to recover absolute voltages. (This property reflects  
148 the fact that  $\hat{K}_{\beta,\alpha}$  and  $\hat{K}_{\alpha,\alpha}$  are correlation matrices rather than covariance matrices.) Also,  
149 note that Equation 11 requires computing a  $T$  by  $T$  matrix, which can become computationally  
150 intractable when  $T$  is very large (e.g. for the patient highlighted in Fig. 2,  $T = 20458799$ ).  
151 However, we may approximate  $Y_{s,k,\beta}$  in a piecewise manner by filling in  $Y_{s,k,\beta}$  in blocks of size  
152  $b$  samples (using the corresponding samples from  $Y_{s,k,\alpha}$ ). In our computations we set  $b = 25000$ .

153 The Super EEG algorithm described above and in Figure 1 allows us to estimate (up to a  
154 constant scaling factor) LFPs for each patient at all arbitrarily chosen locations in the set  $\bar{R}$ ,  
155 *even if we did not record that patient’s brain at all of those locations.*

## 156 Results

157 To test the accuracy with which the Super EEG algorithm reconstructs activity throughout the  
158 brain, we held out each electrode from the full dataset in turn and treated it as unobserved. We  
159 then asked: how closely did each of the Super EEG-reconstructed LFPs match the observed  
160 data? We sought to evaluate both the overall reconstruction accuracy as well as how reconstruc-  
161 tion accuracy varied as a function of implantation location.

162 We first examined raw LFP traces and their associated Super EEG-derived reconstructions.  
163 Figure 2A displays the LFP from the red electrode in Figure 1A, and its associated reconstruc-  
164 tion, during a 5 s time window during one of the patient’s 6 recording sessions. Figure 2B  
165 displays a 2D histogram of the observed versus reconstructed voltages for every sample across  
166 14.2 total hours of recordings from that patient (correlation:  $r = 0.91, p < 10^{-10}$ ). Although the  
167 Super EEG algorithm recovered the recordings from this electrode well, we sought to quantify  
168 the algorithm’s performance across the full dataset.

169 Holding out each electrode from each patient in turn, we computed the average correla-  
170 tion (across recording sessions) between the Super EEG-reconstructed voltage traces and the

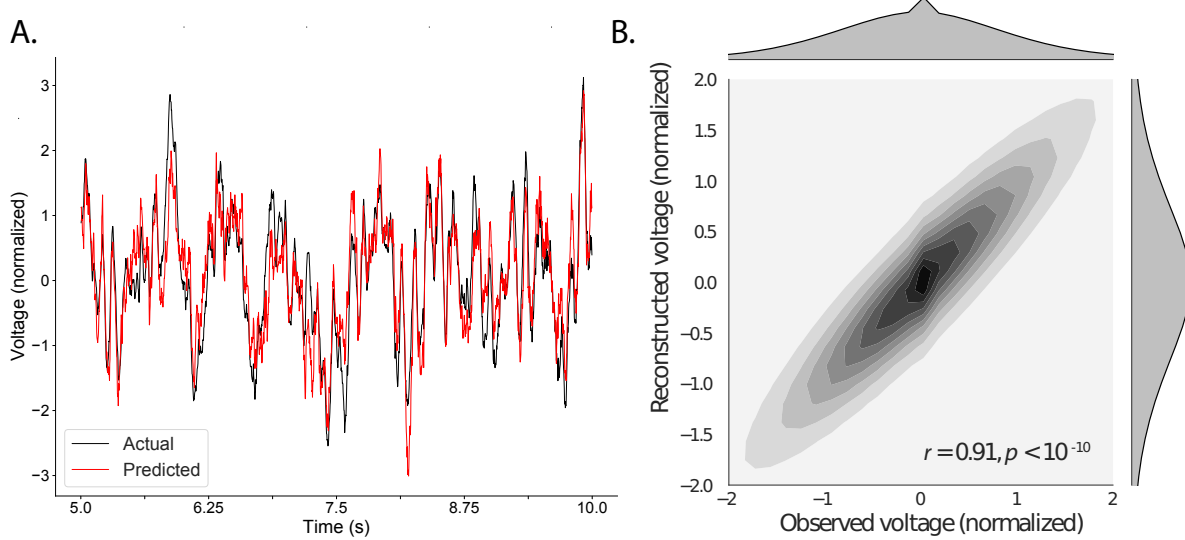


**Figure 2: Observed and reconstructed LFP from a single electrode. A. Example LFP.** A 2 s recording from the blue electrode in Figure 1A is displayed in red, and the reconstructed LFP during the same time window is shown in black. All voltages are plotted in standard deviation units. **B. Observed versus reconstructed voltages over 14.2 hours.** The 2D histogram reflects the relation between distributions of observed versus reconstructed voltages from one patient, across the 14.2 hours of recorded data collected in 6 recording sessions. The correlation reported in the panel is between the observed and reconstructed voltages.

171 observed voltage traces from that electrode. For each reconstruction, we estimated the full-  
172 brain correlation matrix using every *other* patient's data (i.e. every patient except the one who  
173 contributed the to-be-reconstructed electrode data). In our analyses, we then substituted the  
174 average correlation matrix computed after excluding patient  $s$ 's data for  $\hat{K}$  in Equations 9 and  
175 10. This step ensured that the data we were reconstructing could not also be used to estimate  
176 the between-location correlations that drove the reconstructions via Equation 11 (otherwise the  
177 analysis would be circular).

178 We obtained a single correlation coefficient for each electrode location in  $\bar{R}$ , reflecting how  
179 well the Super EEG algorithm was able to recover the recording at that location by incorpo-  
180 rating data across patients (Across shown in black, see Fig. 3A). We also reconstructed activ-  
181 ity for each electrode using a model trained on the remaining electrodes from only that pa-  
182 tient, to account for reconstruction accuracy attributed to volume conductance alone (Within  
183 shown in gray, see Fig. 3A). For the first dataset, we compared these two distributions of  
184 correlation coefficients (paired  $t$ -test between  $z$ -transformed mean correlation coefficients by  
185 patient:  $t(66) = 9.64, p < 10^{-10}$ ). We repeated this analysis on a similar dataset (Fig. 3C)  
186 with similar results (paired  $t$ -test between  $z$ -transformed mean correlation coefficients by pa-  
187 tient:  $t(23) = 6.93, p < 10^{-5}$ ). This is an especially conservative test, given that the Super  
188 EEG reconstructions exclude (from the correlation matrix estimates) all data from the patient  
189 whose data is being reconstructed. Furthermore, we also replicated this finding for each in-  
190 dependent experiment within dataset 2 (Fig. S3 (paired  $t$ -test between  $z$ -transformed mean  
191 correlation coefficients by patient for experiment 1:  $t(23) = 6.23, p < 10^{-5}$  and experiment 2:  
192  $t(23) = 6.62, p < 10^{-5}$ ). That the Super EEG-derived correlations were reliably stronger than  
193 these correlations obtained using a volume conductance null model is exciting for two reasons.  
194 First, it implies that distant electrodes provide additional predictive power to the data recon-  
195 structions beyond the information contained in nearby electrodes. Second, it implies that the

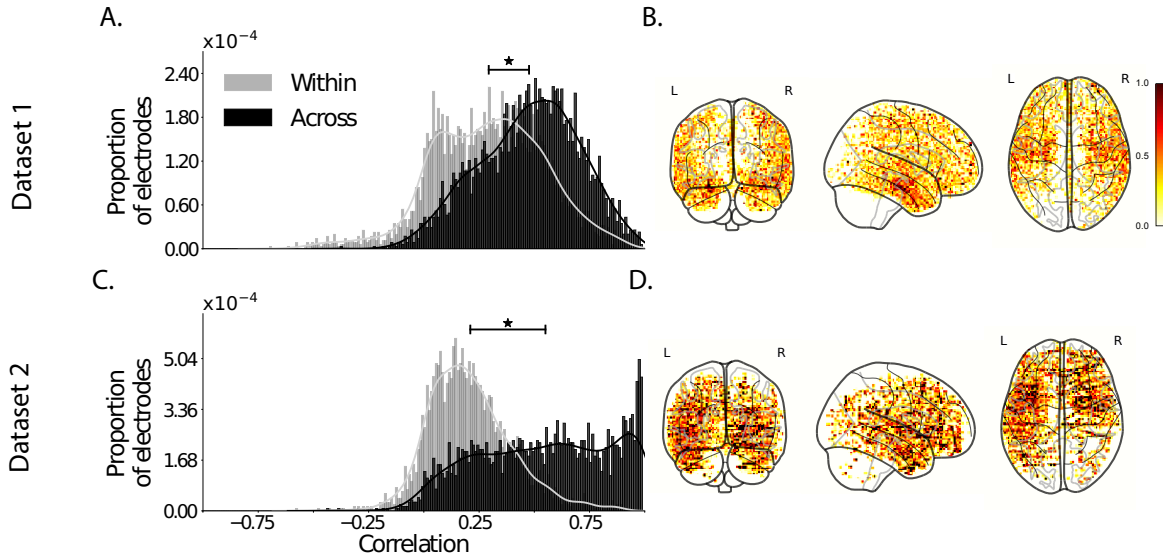


**Figure 3: Reconstruction quality. A. & C. Distributions of correlation coefficients.** Across all electrodes from all patients in the labeled dataset, the panel displays the distribution of correlations between the observed and reconstructed LFP data using models trained on data from all other patients (Across, in black) and all other electrodes from the same patient (Within, in gray). **B. & D. Correlation maps.** The glass brain maps display the average correlation between the observed LFP data and the across-subjects model reconstructed data by location, for each labeled experiment.

196 spatial correlations driving the Super EEG algorithm are, to some extent, shared across people.

197 We were interested in the task specific contributions to the reconstruction accuracy. Each  
 198 patient in the the second dataset participated in two free recall experiments. We ran similar  
 199 analyses for both experiments and found that activity was best reconstructed when limiting the  
 200 training data to within task, as opposed to across task or incorporating data from both tasks (Fig.  
 201 S1 (mean reconstruction accuracy incorporating data within task: 0.55, across task: 0.37, all  
 202 tasks: .50)). Although reconstruction accuracy in the across task analysis was still better than  
 203 the volume conductance model alone (paired *t*-test between *z*-transformed mean correlation  
 204 coefficients by patient:  $t(47) = 5.65, p < 10^{-5}$ ), these results suggests that having a common  
 205 tasks for patients may yield better reconstruction accuracy.

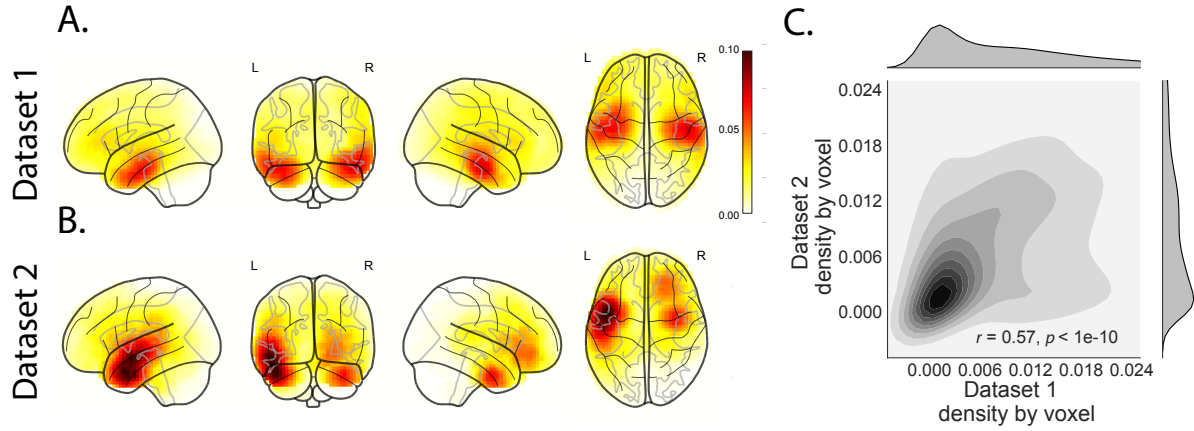


**Figure 4: Sampling density and reconstruction quality.** **A. & B.** The glass brain maps show sampling density by voxel location for dataset 1 and dataset 2. **C.** Correlation of sampling density by voxel location for dataset 1 vs. dataset 2.

We also wondered whether reconstruction quality (measured as the correlation between the observed and reconstructed data) varied with the electrode locations (Fig. 3B & D). In general, reconstruction quality remained high throughout the brain. Although reconstruction accuracy appeared high in the medial temporal lobe, which is a common epileptic focus (and therefore a common target for electrode implantation), we observed a weak but statistically reliable negative correlation between reconstruction quality and electrode density (defined as the proportion of electrodes within 20 MNI units for each location; dataset 1:  $r = -0.07, p < 10^{-5}$ , dataset 2:  $r = -0.16, p < 10^{-10}$ ). This provides some evidence that our reconstruction accuracy results cannot be driven only by volume conductance. Qualitatively, it appeared that the distribution of electrodes was similar across the datasets, suggesting potential commonalities of target locations across patients and similarities in surgical decisions. Indeed, we found a relatively strong correlation between the electrode densities within the two datasets (defined as the proportion of electrodes within 20 MNI units for each 34686 voxels (Fig. 4A, B);  $r = 0.57, p < 10^{-10}$ ).

In addition to exploring how reconstruction quality varies with location, we also wondered whether there might be effects of electrode placements on reconstruction quality. For example,

are there particular implantation locations that yield especially high reconstruction accuracies at other locations throughout the brain? To gain insights into this questions, we computed the average reconstruction correlation for each patient, then computed the average patient reconstruction correlation for any patients who had electrodes within a 20 MNI unit diameter sphere centered on each voxel location. The resulting maps highlight the locations of implanted electrodes from patients whose reconstructions were especially accurate (Fig. 5A and B). We found that the most informative locations were consistent across datasets which lends support to the notion that different electrode location are more informative about activity across patients (Fig. 5C);  $r = 0.22, p < 10^{-10}$ ). The locations in dark red might therefore be good candidate implantation targets for neurosurgeons and neurologists who wish to use Super EEG to reconstruct full-brain electrophysiological signals. The above findings, that one can infer brain activity throughout a person's brain using recordings from a limited number of locations from that person's brain in conjunction with recordings from other people's brains, have deep implications for the structure of brain data. The first implication is that the correlational structure of different people's brain data is largely preserved across individuals. Despite recent evidence that different people have stable but reliably different resting state connectome [5], our results suggest that the correlational structure of different people's brain data is preserved enough across individuals to provide meaningful information.

## Discussion

Super EEG infers full-brain activity patterns by leveraging correlations in those patterns of brain activity within and across people. Although the approach may, in principle, be used to infer brain activity *anywhere* in the brain, the inferences perform slightly better for regions with dense electrode sampling across patients. (Taken to the logical extreme, we could not hope to accurately recover activity patterns from brain areas where no recordings existed from any

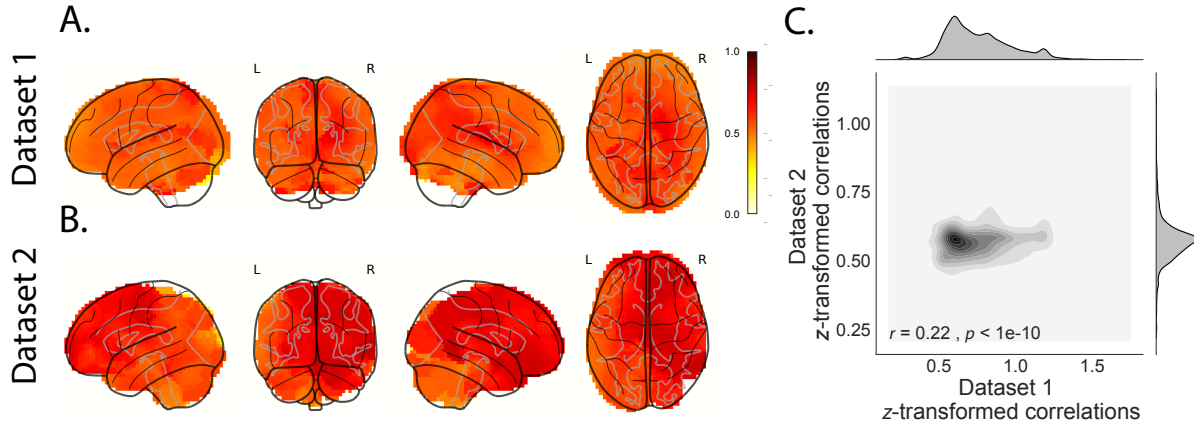


**Figure 5: Most informative electrode locations.** **A. & B.** The glass brain maps displays the average reconstruction correlations (by patient, across all electrodes) for patients with electrodes within a 20 MNI unit diameter sphere centered on each location for dataset 1 and dataset 2. **C.** Correlation between z-transformed correlations by voxel for dataset 1 vs. dataset 2.

patient.) As more data are included in the inference procedure, this suggests that reconstruction accuracy should improve.

A fundamental assumption of the Super EEG algorithm is that the data covariance matrix is stable over time and across people. This is a useful simplification. However, a growing body of evidence from the fMRI community suggests that the data covariance matrix changes in meaningful ways over time (for example, the data covariance matrix changes from moment-to-moment during story listening, serving as a unique “fingerprint” for each moment of the story; further, these task-driven timepoint-specific covariance fingerprints appear to be largely preserved across people [17, 24]). These findings indicate that the full-brain covariance matrix is not stable over time. Other recent work has shown that people’s resting state connectivity matrices may be used to uniquely identify individuals and predict fluid intelligence scores [5]. This indicates that the full-brain covariance matrix is not stable across people. If the fundamental stability assumptions that Super EEG relies on are violated, how can the Super EEG algorithm still accurately recover LFP data? It is important to recognize that the fact that variability (over time

259 or across people) is predictive (e.g. of cognitive states during story listening or fluid intelligence  
260 scores) does not necessarily mean that this variability is large in magnitude. Rather, we have  
261 long known that brain structure is tightly preserved across individuals (and over time, at least  
262 on the timescale of typical clinical and experimental recording sessions), and any functional  
263 changes must occur within the framework of the underlying structural anatomy. Nevertheless,  
264 one could imagine future improvements to the Super EEG approach that leverage resting state  
265 fMRI or structural data [e.g. diffusion tensor imaging (DTI)] to estimate Bayesian priors over  
266 the correlation matrices inferred, in the current framing, using only ECoG data. Further, relax-  
267 ing the assumption that the covariance matrix is stable (over time and/or across people), and/or  
268 incorporating more detailed brain conductance models (e.g. informed by structural MRI scans)  
269 may improve the predictive performance of the approach.

270 One potential limitation of the Super EEG approach is that the above assumption of co-  
271 variance stability across people may be violated even more if different patients are performing  
272 different cognitive tasks. To understand of the extent to which the current findings general-  
273 ize across cognitive tasks, we replicated our initial findings using a dataset in which patients  
274 participated in two tasks, and limited the training data to either within task, across task, or us-  
275 ing both tasks. Since we found the most accurate reconstructions using task-specific data, this  
276 would suggest building up new databases for estimating each task-specific covariance matrix.  
277 Or, using a more sophisticated approach, one could create a hierarchical model whereby each  
278 task-specific covariance matrix was modeled as a perturbation of a “global” task-unspecific  
279 covariance matrix (which could in turn be informed by fMRI or DTI data).

280 A second potential limitation of the Super EEG approach is that it does not provide a nat-  
281 ural means of estimating the precise timing of single-neuron action potentials. Prior work has  
282 shown that gamma band and broadband activity in the LFP may be used to estimate the firing  
283 rates of neurons that underly the population contributing to the LFP [12]. Because Super EEG

284 reconstructs LFPs throughout the brain, one could in principle use gamma or broadband power  
285 in the reconstructed signals to estimate the corresponding firing rates (though not the timings of  
286 individual action potentials).

287 Beyond providing a means of estimating ongoing activity throughout the brain using already  
288 implanted electrodes, our work also has implications for where to place the electrodes in the first  
289 place. Electrodes are typically implanted to maximize coverage of suspected epileptogenic tis-  
290 sue. However, our findings suggest that this approach could be further optimized. Specifically,  
291 one could leverage not only the non-invasive recordings taken during an initial monitoring pe-  
292 riod (as is currently done), but also recordings collected from other patients. We could then ask:  
293 given everything we know about the other patients and from the scalp recordings of this new  
294 patient, where should we place a fixed number of electrodes to maximize our ability to map  
295 seizure foci? As shown in Figure 5, recordings from different locations are differently informa-  
296 tive in terms of reconstructing the spatiotemporal patterns throughout the brain. This property  
297 might be leveraged in decisions about where to surgically implant electrodes in future patients.

298 **Concluding remarks**

299 Over the past several decades, neuroscientists have begun to leverage the strikingly profound  
300 mathematical structure underlying the brain’s complexity to infer how our brains carry out com-  
301 putations to support our thoughts, actions, and physiological processes. Whereas traditional  
302 beamforming techniques rely on geometric source-localization of signals measured at the scalp,  
303 here we propose an alternative approach that leverages the rich correlational structure of a large  
304 dataset of human intracranial recordings. In doing so, we are one step closer to observing, and  
305 perhaps someday understanding, the full spatiotemporal structure of human neural activity.

306 **Code availability**

307 We have released an open-source SuperEEG Python toolbox. All of the code used in this  
308 manuscript is on GitHub, and the code may be shared using a GitHub account accessible to  
309 the reviewers upon request.

310 **Data availability**

311 The dataset analyzed in this study was generously shared by Michael J. Kahana. A portion of  
312 the dataset may be downloaded [here](#).

313 **Acknowledgements**

314 We are grateful for useful discussions with Luke J. Chang and Matthijs van der Meer. We are  
315 also grateful to Michael J. Kahana for generously sharing the ECoG dataset we analyzed in our  
316 paper, which was collected under NIMH grant MH55687 to MJK. Our work was also supported  
317 in part by NSF EPSCoR Award Number 1632738. The content is solely the responsibility of the  
318 authors and does not necessarily represent the official views of our supporting organizations.

319 **Author Contributions**

320 J.R.M conceived and initiated the project. L.L.W.O. and A.C.H. performed the analyses. J.R.M.  
321 and L.L.W.O. wrote the manuscript.

322 **Author Information**

323 Reprints and permissions information is available at [www.nature.com/reprints](http://www.nature.com/reprints). The authors de-  
324clare no competing financial interests. Readers are welcome to comment on the online version  
325 of the paper. Publisher's note: Springer Nature remains neutral with regard to jurisdictional

326 claims in published maps and institutional affiliations. Correspondence and requests for mate-  
327 rials should be addressed to J.R.M. ([jeremy.r.manning@dartmouth.edu](mailto:jeremy.r.manning@dartmouth.edu)).

## 328 References and Notes

- 329 [1] Becker, C. O., Pequito, S., Pappas, G. J., Miller, M. B., adn D S Bassett, S. T. G., and  
330 Preciado, V. M. (2018). Spectral mapping of brain functional connectivity from diffusion  
331 imaging. *Scientific Reports*, 8(1411):<https://www.doi.org/10.1038/s41598-017-18769-x>.
- 332 [2] Casey, B. J., Giedd, J. N., and Thomas, K. M. (2000). Structural and functional brain  
333 development and its relation to cognitive development. *Biological Psychology*, 54(1–3):241–  
334 257.
- 335 [3] Ezzyat, Y., Kragel, J. E., Burke, J. F., Levy, D. F., Lyalenko, A., Wanda, P., O’Sullivan, L.,  
336 Hurley, K. B., Busygin, S., Pedisich, I., Sperling, M. R., Worrell, G. A., Kucewicz, M. T.,  
337 Davis, K. A., Lucas, T. H., Inman, C. S., Lega, B. C., Jobst, B. C., Sheth, S. A., Zaghloul, K.,  
338 Jutras, M. J., Stein, J. M., Das, S. R., Gorniak, R., Rizzuto, D. S., and Kahana, M. J. (2017).  
339 Direct brain stimulation modulates encoding states and memory performance in humans.  
340 *Current Biology*, 27:1–8.
- 341 [4] Ezzyat, Y., Wanda, P. A., Levy, D. F., Kadel, A., Aka, A., Pedisich, I., Sperling, M. R.,  
342 Sharan, A. D., Lega, B. C., Burks, A., Gross, R. E., Inman, C. S., Jobst, B. C., Goren-  
343 stein, M. A., Davis, K. A., Worrell, G. A., Kucewicz, M. T., Stein, J. M., Gorniak, R.,  
344 Das, S. R., Rizzuto, D. S., and Kahana, M. J. (2018). Closed-loop stimulation of tem-  
345 poral cortex rescues functional networks and improves memory. *Nature Communications*,  
346 9(365):<https://www.doi.org/10.1038/s41467-017-02753-0>.
- 347 [5] Finn, E. S., Shen, X., Scheinost, D., Rosenberg, M. D., Huang, J., Chun, M. M., Pa-

- 348 pademetrис, X., and Constable, R. T. (2015). Functional connectome fingerprinting: identi-  
349 fying individuals using patterns of brain connectivity. *Nature Neuroscience*, 18:1664 – 1671.
- 350 [6] Horak, P. C., Meisenhelter, S., Song, Y., Testorf, M. E., Kahana, M. J., Viles, W. D., Bu-  
351 jarski, K. A., Connolly, A. C., Robbins, A. A., Sperling, M. R., Sharan, A. D., Worrell, G. A.,  
352 Miller, L. R., Gross, R. E., Davis, K. A., Roberts, D. W., Lega, B., Sheth, S. A., Zaghloul,  
353 K. A., Stein, J. M., Das, S. R., Rizzuto, D. S., and Jobst, B. C. (2017). Interictal epileptiform  
354 discharges impair word recall in multiple brain areas. *Epilepsia*, 58(3):373–380.
- 355 [7] Jahanshad, N., Kochunov, P. V., Sprooten, E., Mandl, R. C., Nichols, T. E., Almasy, L.,  
356 Blangero, J., Brouwer, R. M., Curran, J. E., de Zubicaray, G. I., Duggirala, R., Fox, P. T.,  
357 Hong, L. E., Landman, B. A., Martin, N. G., McMahon, K. L., Medland, S. E., Mitchell,  
358 B. D., Olvera, R. L., Peterson, C. P., Starr, J. M., Sussmann, J. E., Toga, A. W., Wardlaw,  
359 J. M., Wright, M. J., Pol, H. E. H., Pastin, M. E., McIntosh, A. M., Deary, I. J., Thompson,  
360 P. M., and Glahn, D. C. (2013). Multi-site genetic analysis of diffusion images and voxel-  
361 wise heritability analysis: A pilot project of the enigma-dti working group. *NeuroImage*,  
362 81(1):455–469.
- 363 [8] Kragel, J. E., Ezzyat, Y., Sperling, M. R., Gorniak, R., Worrell, G. A., Berry, B. M., Inman,  
364 C., Lin, J.-J., Davis, K. A., Das, S. R., Stein, J. M., Jobst, B. C., Zaghloul, K. A., Sheth,  
365 S. A., Rizzuto, D. S., and Kahana, M. J. (2017). Similar patterns of neural activity predict  
366 memory formation during encoding and retrieval. *NeuroImage*, 155:70–71.
- 367 [9] Kucewicz, M. T., Berry, B. M., Kremen, V., Brinkmann, B. H., Sperling, M. R., Jobst,  
368 B. C., Gross, R. E., Lega, B., Sheth, S. A., Stein, J. M., Das, S. R., Gorniak, R., Stead, S. M.,  
369 Rizzuto, D. S., Kahana, M. J., and Worrell, G. A. (2017). Dissecting gamma frequency  
370 actiivty during human memory processing. *Brain*, 140:1337–1350.

- 371 [10] Kucewicz, M. T., Berry, B. M., Miller, L. R., Khadjevand, F., Ezzyat, Y., Stein, J. M.,  
372 Kremen, V., Brinkmann, B. H., Wanda, P., Sperling, M. R., Gorniak, R., Davis, K. A., Jobst,  
373 B. C., Gross, R. E., Lega, B., Gompel, J. V., Stead, S. M., Rizzuto, D. S., Kahana, M. J.,  
374 and Worrell, G. A. (2018). Evidence for verbal memory enhancement with electrical brain  
375 stimulation in the lateral temporal cortex. *Brain*, 141(4):971–978.
- 376 [11] Lin, J.-J., Rugg, M. D., Das, S., Stein, J., Rizzuto, D. S., Kahana, M. J., and Lega, B. C.  
377 (2017). Theta band power increases in the posterior hippocampus predict successful episodic  
378 memory encoding in humans. *Hippocampus*, 27:1040–1053.
- 379 [12] Manning, J. R., Jacobs, J., Fried, I., and Kahana, M. J. (2009). Broadband shifts in LFP  
380 power spectra are correlated with single-neuron spiking in humans. *The Journal of Neuro-  
381 science*, 29(43):13613–13620.
- 382 [13] Manning, J. R., Polyn, S. M., Baltuch, G., Litt, B., and Kahana, M. J. (2011). Oscillatory  
383 patterns in temporal lobe reveal context reinstatement during memory search. *Proceedings  
384 of the National Academy of Sciences, USA*, 108(31):12893–12897.
- 385 [14] Manning, J. R., Ranganath, R., Norman, K. A., and Blei, D. M. (2014). Topographic  
386 factor analysis: a Bayesian model for inferring brain networks from neural data. *PLoS One*,  
387 9(5):e94914.
- 388 [15] Manning, J. R., Sperling, M. R., Sharan, A., Rosenberg, E. A., and Kahana, M. J. (2012).  
389 Spontaneously reactivated patterns in frontal and temporal lobe predict semantic clustering  
390 during memory search. *The Journal of Neuroscience*, 32(26):8871–8878.
- 391 [16] Manning, J. R., Zhu, X., Willke, T. L., Ranganath, R., Stachenfeld, K., Hasson, U., Blei,  
392 D. M., and Norman, K. A. (2018). A probabilistic approach to discovering dynamic full-  
393 brain functional connectivity patterns. *NeuroImage*.

- 394 [17] Manning, J. R., Zhu, X., Willke, T. L., Ranganath, R., Stachenfeld, K., Simony, E., Has-  
395 son, U., Blei, D. M., and Norman, K. A. (2017). A probabilistic approach to discovering  
396 dynamic full-brain functional connectivity patterns. *bioRxiv*, page 106690.
- 397 [18] Mori, S., Oishi, K., Jiang, H., Jiang, L., Li, X., Akhter, K., Hua, K., Faria, A. V., Mah-  
398 mood, A., Woods, R., Toga, A. W., Pike, G. B., Neto, P. R., Evans, A., Zhang, J., Huang, H.,  
399 Miller, M. I., van Zijl, P., and Mazziotta, J. (2008). Stereotaxic white matter atlas based on  
400 diffusion tensor imaging in an icbm template. *NeuroImage*, 40(2):570–582.
- 401 [19] Rasmussen, C. E. (2006). *Gaussian processes for machine learning*. MIT Press.
- 402 [20] Sawyer, R. J. (1995). *The Terminal Experiment*. HarperPrism.
- 403 [21] Sederberg, P. B., Kahana, M. J., Howard, M. W., Donner, E. J., and Madsen, J. R. (2003).  
404 Theta and gamma oscillations during encoding predict subsequent recall. *Journal of Neuro-  
405 science*, 23(34):10809–10814.
- 406 [22] Sederberg, P. B., Schulze-Bonhage, A., Madsen, J. R., Bromfield, E. B., Litt, B., Brandt,  
407 A., and Kahana, M. J. (2007a). Gamma oscillations distinguish true from false memories.  
408 *Psychological Science*, 18(11):927–932.
- 409 [23] Sederberg, P. B., Schulze-Bonhage, A., Madsen, J. R., Bromfield, E. B., McCarthy, D. C.,  
410 Brandt, A., Tully, M. S., and Kahana, M. J. (2007b). Hippocampal and neocortical gamma  
411 oscillations predict memory formation in humans. *Cerebral Cortex*, 17(5):1190–1196.
- 412 [24] Simony, E., Honey, C. J., Chen, J., and Hasson, U. (2016). Uncovering stimulus-locked  
413 network dynamics during narrative comprehension. *Nature Communications*, 7(12141):1–  
414 13.

- 415 [25] Solomon, E. A., Gross, R., Lega, B., Sperling, M. R., Worrell, G., Sheth, S. A., Zaghloul,  
416 K. A., Jobst, B. C., Stein, J. M., Das, S., Gorniak, R., Inman, C., Seger, S., Kragel, J. E.,  
417 Rizzuto, D. S., and Kahana, M. J. (2018). Mtl functional connectivity predicts stimulation-  
418 induced theta power. *Nature Communications*, In press.
- 419 [26] Sporns, O. and Betzel, R. F. (2016). Modular brain networks. *Annual Review of Psychol-*  
420 *ogy*, 67:613–640.
- 421 [27] Talairach, J. and Tournoux, P. (1988). *Co-planar stereotaxic atlas of the human brain*.  
422 Verlag, Stuttgart.
- 423 [28] Turk-Browne, N. B. (2013). Functional interactions as big data in the human brain. *Sci-*  
424 *ence*, 342:580–584.
- 425 [29] Weidemann, C. T., Kragel, J. E., Lega, B. C., Worrell, G. A., Sperling, M. R., Sharan,  
426 A. D., Jobst, B. C., Khadjevand, F., Davis, K. A., Wanda, P. A., Kadel, A., Rizzuto, D. S.,  
427 and Kahana, M. J. (2018). Neural activity reveals interactions between episodic and semantic  
428 memory systems during retrieval. *Journal of Experimental Psychology: General*, In press.
- 429 [30] Yeo, B. T. T., Krienen, F. M., Sepulcre, J., Sabuncu, M. R., Lashkari, D., Hollinshead, M.,  
430 Roffman, J. L., Smoller, J. W., Zollei, L., Polimieni, J. R., Fischl, B., Liu, H., and Buckner,  
431 R. L. (2011). The organization of the human cerebral cortex estimated by intrinsic functional  
432 connectivity. *Journal of Neurophysiology*, 106(3):1125–1165.